

Traffic Induced Reflective Cracking on Pavements with Geogrid-Reinforced Asphalt Concrete Overlay

TRB Paper #03-2370

Submitted for Publication and Presentation at the
82th Annual TRB Meeting, January 2003

Chen-Ming Kuo
Associate Professor of Department of Civil Engineering
National Cheng Kung University
#1, University Road
Tainan, 70101, Taiwan
TEL: 886-6-2757575 ex. 63170
E-mail: ckuo@mail.ncku.edu.tw

Tsung-Rung Hsu
Research Assistant of Department of Civil Engineering
National Cheng Kung University
#1, University Road
Tainan, 70101, Taiwan

Submission date: 2002/7/24

Word count: 6915

Abstract

The progress of reflective cracking on geogrid-reinforced asphalt overlay on cracked rigid pavements was investigated by iterative analysis of three-dimensional finite element models. The model consisted of Winkler subgrade, jointed concrete slabs, bonded interfaces between layers, equivalent geogrid layers with membrane elements, and asphalt overlays. Cracking path was predicted according to fatigue life prediction of all parts of the model. The repetitions at all cracking stages that compose the entire cracking process were summed up to estimate the service life of geogrid-reinforced overlay. Geogrid position, overlay thickness, PCC slab integrity, and asphalt concrete stiffness were varied to model 18 analysis cases. Three basic types of reflective cracking propagation were all identified with the 18 FEM analyses. Most cases cracked from bottom, whereas top-down cracking were found likely happening with the condition of relatively soft overlay stiffness or very thick overlay. Placing the geogrid at the 1/3 depth of overlay thickness had the maximum predicted service life. The strength of geogrid does not affect overlay performance significantly.

Keywords :

Overlay
Geogrid
Reflective cracking
Top-down cracking
Fatigue

INTRODUCTION

Reflective cracking has been one of the major concerns for asphalt concrete overlay on deteriorated Portland Cement concrete pavements. It is widely believed that traffic repetitions and cyclic temperature variations are the causes of reflective cracking (1). The cracking mechanism and growth inspired plenty studies in order to remedy the problem. Eltahan and Lytton derived crack initiation and propagation formula with fracture mechanics (2). Later, Rigo et al. utilized a two-dimensional (2-D) finite element program to model overlay pavements subjected to truck wheels and temperature variations (3). The cracks were traced by iterative FEM analysis by removing the elements of maximum stress. Castel et al. predicted crack growth rate with maximum strains and found bottom-up cracking is more likely found than top-down cracking be (4). By solving ODE with computer programs, Lytton et al. predicted the time of crack initiation and the associated traffic volume (5).

Thick overlay was once considered to prevent bottom-up reflective cracks. Yet, Uhlmeier et al. investigated thick overlay and found cracks starting at surface and propagate downward (6). Sha also noticed top-down reflective cracking for thick overlay according to field observations in China (7). The number of cracks decreased with increasing strength and thickness of asphalt concrete.

As geosynthetic materials prevail, asphalt concrete reinforced with geogrid was tried in order to hinder initiation of reflective cracking. The effects of geogrid were explained in three aspects, 1. providing constrains at the crack tips; 2. absorbing cracking energy to retard propagation; 3. producing interlocking between geogrid and aggregate to reduce stress concentration (8). However, it is hard to learn the behavior of reinforced asphalt overlay in the lab because of difficulties in preparing sample beams of composite layers resembling the overlay structure. The field performance of geogrid-reinforced overlay was varied because it depends on construction procedures, position of geogrid, interfacial treatment between layers, and weather conditions. In 1986, Texas Transportation Institute conducted lab tests with overlay tester to investigate cracks and fatigue life of a sample asphalt concrete beam with GlasGrid in the mid-depth. The lab tests concluded that geogrid-reinforced asphalt concrete beam outperformed a 25% thicker plain asphalt concrete beam. Furthermore, three types of reflective cracking were found, as shown in **FIGURE 1** (9). Guo studied geogrid-reinforced asphalt overlay in the field in 1990 and found that the glass fiber grid placed at the bottom of overlay was effective in limiting cracks near the interface and increase 42% of bending strength and 80% of fatigue life (10). Fuji Yugo conducted field tests and concluded that thick asphalt overlay reinforced with geogrid did decrease surface deflections; and two layers of geogrid are even more effective than single layer (11).

To understand the behavior of geogrid-reinforced asphalt overlay structure, this research was designated to reveal the crack growth and the effect of parameters of overlay structure on fatigue life from the truck loading point of view.

FEM MODELS

The finite element analyses were based on the three-dimensional (3-D) model developed with ABAQUS package (12). The model was well validated for analysis of concrete pavement, asphalt pavement, and composite pavement with geogrid-reinforced asphalt overlay on concrete slabs (13,14). **FIGURE 2** shows the overview of 3-D finite element model of the overlay structure analyzed in this study. Due to extreme stress fluctuation due to wheels passing in the vicinity area of joint/crack in the old PCC pavement and bottom of overlay, the a dual axle loading was placed at the position right above the PCC slab joint/crack. The asphalt overlay was modeled with 20-node brick elements. Two layers of brick elements were separated by geogrid elements. By adjusting the thickness of upper layer and lower layer, the position of geogrid in the overlay could be varied in the model. Meanwhile, uniaxial creep test of asphalt concrete is necessary to simulate viscoelastic behavior.

The geogrid was modeled with membrane elements with the same thickness as glass fiber grids. However, the strength of this membrane is much stiffer than real geogrid if the actual Young's moduli of geogrid materials were used. This is because the cross section area of membrane elements is much larger than the that of real geogrid. As shown in **FIGURE 3**, the effective modulus was derived to compensate the large cross section of membrane elements.

Old concrete slabs were modeled with 20-node brick elements. Joint/crack was simulated by setting the elements at the location with low elastic modulus. Various condition of joint/crack can be manipulated with the low elastic modulus. The load transfer efficiency of joint/crack was calculated with Eq.1. Trial analysis shows that 66% of load transfer efficiency could be achieved if the elastic modulus of joint elements was set 10% of normal modulus of Portland cement concrete.

$$LTE_{\delta} = \frac{dU}{dL} \times 100\% \quad \text{Eq.1}$$

where

LTE_{δ} : Load transfer efficiency (with respect to slab deflection)

dU : Maximum deflection of the unloaded slab along the joint

dL : Maximum deflection of the loaded slab along the joint

Interface elements were used to define the contact conditions between layers. Three contact interfaces made this model a very complicated pavement model. The contact of upper layer of overlay and geogrid sheet forms Interface No.1. Downside of geogrid contacts with lower layer of overlay generating Interface No.2. These two interfaces are both governed by the vertical and horizontal adhesion and friction coefficient between asphalt concrete and geogrid. Further down, the contact between bottom of lower layer and top of concrete slabs forms Interface No.3, which depends on the bonding of asphalt on concrete and friction coefficient between asphalt and concrete.

The pavement support was modeled with continuous springs as Winkler foundation to save computer resources. The values of material properties used in the analysis are listed in **TABLE 1**.

CRACK PREDICTION

It was assumed that crack initiates at the critical point where the computed stress exceeds the ultimate strength or where the predicted fatigue life is the shortest in the entire model. After the critical point was determined, the FEM model was modified by setting the material property at the critical point with a low modulus to simulate cracks. If the critical point was located in interface, the bonding was removed and friction was left the only force in interface. The analysis was conducted with the modified model to find the next critical point. The process was iterated until the crack reached surface. **FIGURE 4** shows details of the iteration scheme.

Fatigue models and material ultimate strengths are the key factors for the accuracy of crack growth proposed above. Ideally, every interface and material at specific environment condition has different relationship between stress/strain level and fatigue life, which require fatigue tests in laboratory. However, laboratory tests of various bonding interface and overlay materials were beyond the scope of this study. Furthermore, there is no ready-to-use or relevant fatigue model in literature for debonding between geogrid and asphalt concrete and between asphalt concrete and Portland cement concrete. Hence, the popular fatigue formula, listed in **TABLE 2**, for PCC and AC were used for feasibility study of the proposed scheme. It should be noted that stress fatigue model and strain fatigue model of AC were both considered because the failure criteria of AC in high temperature and low temperature are generally controlled by strain and stress respectively.

The factorial matrix of parameters considered in the study is listed in **TABLE 3**. Three types of cracking path were identified according to the prediction results.

Type I :

As shown in **FIGURE 5**, debonding occurred first between geogrid and overlay AC. Then, cracks developed from bottom of overlay and propagated all the way through overlay, and reached road surface. This cracking pattern was found in Case 3, 4, 5, 7, 8, 10, 11, 13, 14, 15, 16, 18.

Type II :

As shown in **FIGURE 6**, debonding occurred first between geogrid and PCC slabs. Then, the cracking energy was trapped by the interfacial debonding in interface No.3 until a significant debonded region was formed. Several cracks were then developed from the bottom of overlay along PCC joint/crack. Finally, the crack located beneath the loading wheel penetrated upward and reached road surface. This cracking pattern was only found in Case 12, in which geogrid was directly placed on PCC slab.

Type III :

As shown in **FIGURE 7**, top-down cracking pattern was identified in Case 1, 2, 6, 9, and 17. At the loading position, crack developed from bottom of lower layer of AC overlay. Then, debonding of interface No.2 developed transversely along PCC slab joint/crack. Finally, the upper layer of AC overlay started to crack from top and propagated towards interface No.1.

Several findings were obtained by examining the condition of each case and its cracking pattern.

1. Load transfer efficiency (LTE) of PCC slab joint/crack is significant to reflective cracking pattern. High LTE reduces stress concentration at the overlay bottom along the joint, hence more likely causes top-down reflective cracking.
2. Overlay thickness is another key factor causing top-down cracking. Thick overlay effectively alleviates stress/strain at overlay bottom, yet the stress/strain around load prints becomes critical cracking area.

3. The ultimate strength of geogrid material was less likely alters the cracking pattern.
4. High temperature softens AC overlay and causes top-down cracking even though overlay thickness is not very thick.

FATIGUE LIFE PREDICTION

Quantitative comparison of the analyzed cases is another important issue in exploring the interaction effects of geogrid position, overlay thickness, and other related pavement parameters. Fatigue life prediction is generally adopted in pavement study to obtain relatively superior structures. The simulation results of crack growth were transferred into service life by fatigue models.

It is more complicated to calculate the accumulated fatigue life of pavements with growing cracks than general fatigue prediction without cracks.

The stress/strain computed by each FEM analysis was substituted into the associated fatigue models to calculate the allowable repetitions at the stage. The critical element at the stage was found with fatigue life, $N_{i,i}$, where i denotes the stage number. In the meantime, certain percentage of fatigue life being consumed at the critical element in the previous stages was estimated. The total traffic repetitions that the overlay can take before cracks appearing on road surface can be obtained with Eq.2 and Eq.3 (1).

$$n_1 = N_{1,1}, \quad n_i = N_{i,i} \cdot \left(1 - \sum_{j=1}^{i-1} \frac{n_j}{N_{i,j}} \right) \quad \text{Eq.2}$$

$$n_{sum} = \sum_{i=1} n_i \quad \text{Eq.3}$$

where

- n_i : The repetitions in iteration stage i
- $N_{i,j}$: The allowable repetition of the critical element at stage i in the previous stage j .
- N_{sum} : The total repetitions for the reflective crack reaching overlay surface

FIGURE 8 compares the predicted repetitions for Case 1, 2, 3, and 4. It shows that overlays on the old pavements with high LTE have longer service life. From the geogrid material point of view, high strength geogrid is advantageous for the badly cracked slabs. In other words, it is important to choose proper geogrid if the old pavement is severely deteriorated.

The geogrid position cause significant variation of service life as shown in **FIGURE 9**. If geogrid is placed directly on cracked PCC slab, the section only lasts one third of the case placing geogrid at $1/3h$ above PCC slab surface. **FIGURE 10** further illustrates tensile strain variation of AC overlays with different geogrid positions. Geogrid position changes distribution of tensile strains between upper layer and lower layer of AC overlay. The $1/3h$ position evenly distributes deformation energy to two layers and lowers the strain level to result in long service life.

Overlay thickness is another key factor affecting service life. As shown in **FIGURE 11**, the service life remarkably increases with overlay thickness. The influence of ambient temperature on overlay service life can be examined by comparing Case 3 and 17. In 26°C , the overlay was expected to carry 5.2×10^6 repetitions. The capacity of the same overlay design could be reduced to 0.43×10^6 in the condition of 58°C , which is less than tenth of the capacity in 26°C .

Comprehensive comparison for all analyzed cases is shown as **FIGURE 12**. Case 8 has highest predicted life because of very thick overlay. Although it is not practical to design a 229mm AC overlay, this case still reveal the fact that increasing overlay thickness is the most effective means to increase service life, even with no geogrid reinforcement. However, this conclusion does not imply ineffectiveness of geogrid. The overlay thickness of Case 5 is only 67% of Case 4, but Case 5 has better predicted service life because of stronger geogrid than Case 4. In addition, comparing Case 3 and Case 7, introducing geogrid increases 16% service life.

CONCLUSIONS

Three-dimensional finite element model of composite pavement composing of Winkler foundation, concrete slabs with joints, lower layer of asphalt overlay, reinforcing geogrid, upper layer of overlay was built to investigate the mechanism of reflective cracking and propagation path. A procedure of tracing crack growth was developed by fatigue prediction and iteration of FEM analysis. Three basic types of reflective cracking

were all identified in the 18 analysis cases that take severity of PCC crack, geogrid position, geogrid strength, ambient temperature, and overlay thickness into consideration. Finally, a procedure of damage accumulation during crack growth was introduced, and the results of analysis cases were quantified with the predicted service life. Several findings can be summarized as follows.

1. Geogrid is effective in reinforcing asphalt overlay to postpone appearance of reflective cracking.
2. Placing geogrid at 1/3 design overlay thickness divides the overlay into lower layer and upper layer. This design is advantageous with lower layer serving as leveling layer that ensures good seating and bonding of geogrid. It also evenly distributes deformation energy into the two sub-layers.
3. Based on the simulations in this study, overlay deterioration starts with interface debonding in most situations. Cracks in AC overlay then initiate from the contact points with PCC joint/crack and propagate all the way up to road surface.
4. Top-down cracking pattern was found in two situations. First, the relative stiffness of overlay respective to PCC slabs is low, e.g., joint/crack with high LTE or soft asphalt concrete at high temperature. The other situation for top-down cracking is very thick overlay.
5. The strength of geogrid significantly affects the predicted service life if joint/crack of PCC slabs has very low LTE.
6. Finally, the proposed procedures have been proven feasible for tracing reflective cracking and service life prediction. The prediction accuracy can be improved provided that proper fatigue models and exact material strength are available.

List of Tables and Figures

TABLE 1 Model inputs of loading and material property

TABLE 2 Fatigue formula adopted in the analysis

TABLE 3 Combinations of pavement parameters analyzed

FIGURE 1 Three basic types of reflective cracking (9)

FIGURE 2 Sketch of finite element model of composite pavement

FIGURE 3 Transformed geogrid for FEM model

FIGURE 4 Flow chart of crack path prediction

FIGURE 5 Type I cracking path

FIGURE 6 Type II cracking path

FIGURE 7 Type III cracking path

FIGURE 8 Service life comparison of Case 1, 2, 3, 4

FIGURE 9 Service life comparison of various geogrid position

FIGURE 10 Tensile strains of various geogrid positions

FIGURE 11 Service life comparisons of various geogrid position

FIGURE 12 Service life comparisons of 10 analysis cases

TABLE 1 Model inputs of loading and material property

Layer Materials			
	Young's modulus, GPa	Poison's ratio	Unit weight, kN/m ³
Asphalt concrete	1.02 (26°C); 0.24 (58°C)	0.35	22.8
Glass fiber geogrid	69	0.04	1.7
Polypropylene geogrid	1.8	0.04	1.7
PCC	27.6	0.15	23.6
Loading			
Axle loading	2×36.8 kN		
Contact pressure	465 kPa		
Wheel spacing	1.8 m		
Interface			
	Friction coefficient		
Interface No.1	5		
Interface No.2	5		
Interface No.3	8		
Subgrade			
Modulus of reaction	54 MPa/m		

TABLE 2 Fatigue formula adopted in the analysis

Material	Fatigue formula	Ultimate strength
Overlay AC	$N_{AC}^{\sigma} = 1.33 \times 10^9 \left(\frac{1}{\sigma} \right)^{2.79}$; $N_{AC}^{\varepsilon} = 5.13 \times 10^{-4} \left(\frac{1}{\varepsilon} \right)^{2.33}$ [15]	26°C : 1.37 MPa
		58°C :
PCC	$\log N = 11.78 - 12.11 \frac{\sigma}{MR}$ [16]	4.24 MPa
Geogrid	$\frac{\sigma}{2152} = 1 - \frac{1}{11} \log N_f$ [17]	2160 MPa
Interface	Fatigue formula	Friction coefficient
Geogrid/AC	$\tau = -73.22 \times \ln(N_f) + 1327.8$ (Revised from [18])	5
AC/PCC	$N = 8.1 \times 10^{-5} \times \left(\frac{1}{\varepsilon} \right)^{3.92}$ [19]	8

TABLE 3 Combinations of pavement parameters analyzed

No.	Load Transfer Efficiency	Geogrid		AC overlay Thickness (h)	Temperature	Crack type
		Material	Position*			
1	66%	Glass fiber	$1/3 h$	114 mm	26°C	III
2	66%	Polypropylene	$1/3 h$	114 mm	26°C	III
3	5%	Glass fiber	$1/3 h$	114 mm	26°C	I
4	5%	Polypropylene	$1/3 h$	114 mm	26°C	I
5	5%	Glass fiber	$1/3 h$	76 mm	26°C	I
6	5%	Glass fiber	$1/3 h$	229 mm	26°C	III
7	5%	–	–	114 mm	26°C	I
8	5%	–	–	229 mm	26°C	I
9	5%	–	–	381 mm	26°C	III
10	5%	Glass fiber	$1/2 h$	114 mm	26°C	I
11	5%	Glass fiber	$1/9 h$	114 mm	26°C	I
12	5%	Glass fiber	0h	114 mm	26°C	II
13	0	Glass fiber	$1/9 h$	114 mm	26°C	I
14	5%	Glass fiber	$1/3 h$	25 mm	58°C	I
15	5%	Glass fiber	$1/3 h$	51 mm	58°C	I
16	5%	Glass fiber	$1/3 h$	76 mm	58°C	I
17	5%	Glass fiber	$1/3 h$	114 mm	58°C	III
18	5%	Glass fiber	$1/3 h$	114 mm	26°C	I

* Distance from bottom of overlay AC

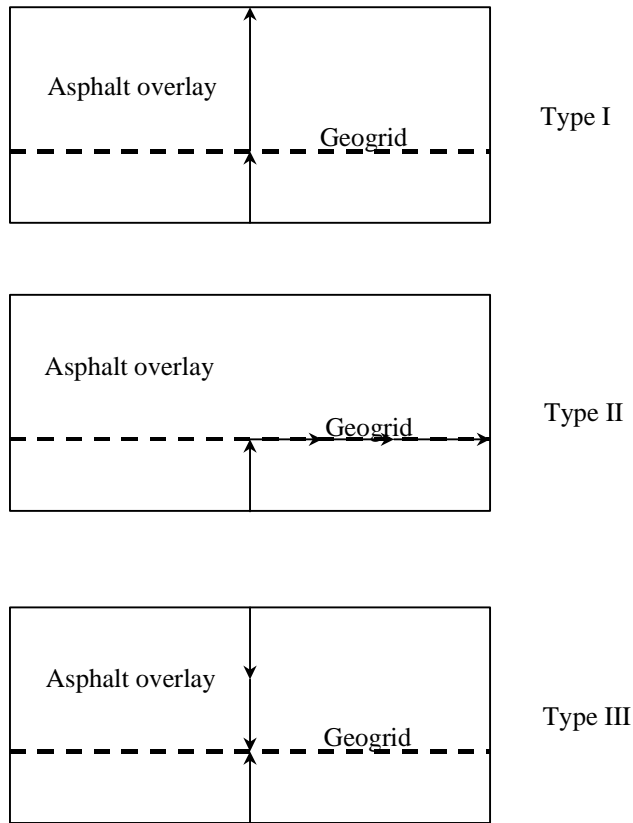


FIGURE 1 Three basic types of reflective cracking (9)

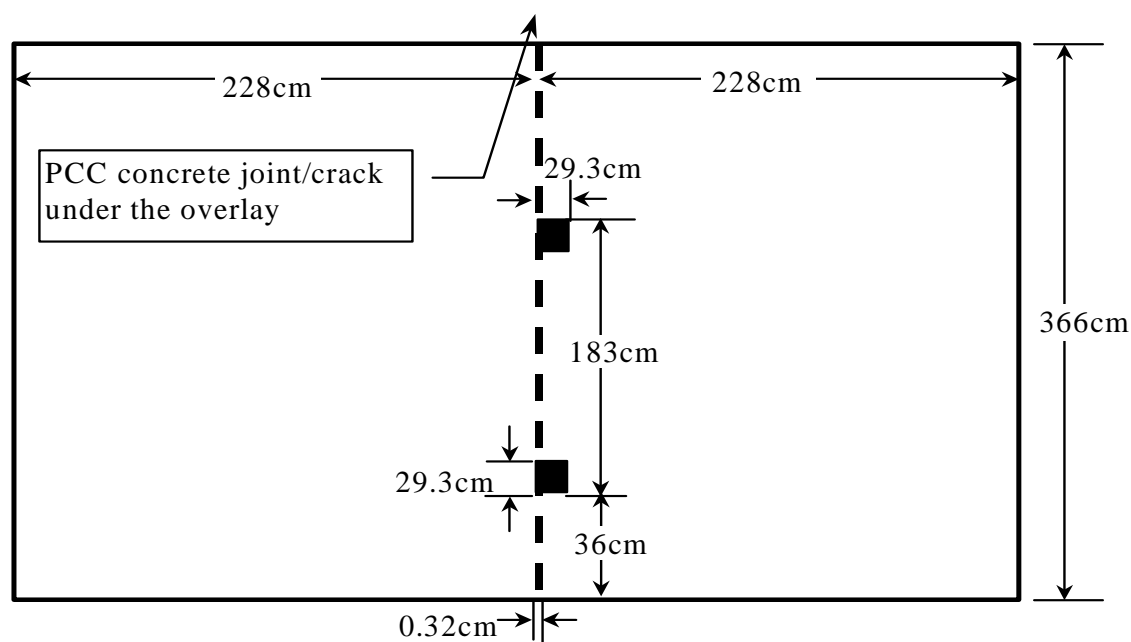
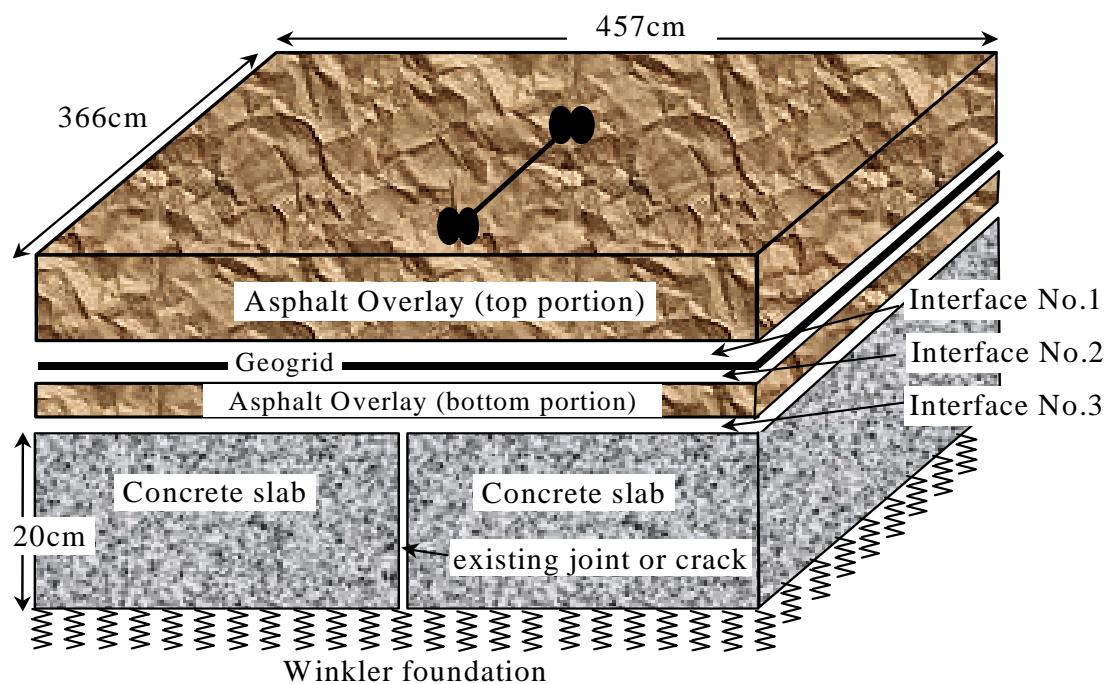


FIGURE 2 Sketch of finite element model of composite pavement

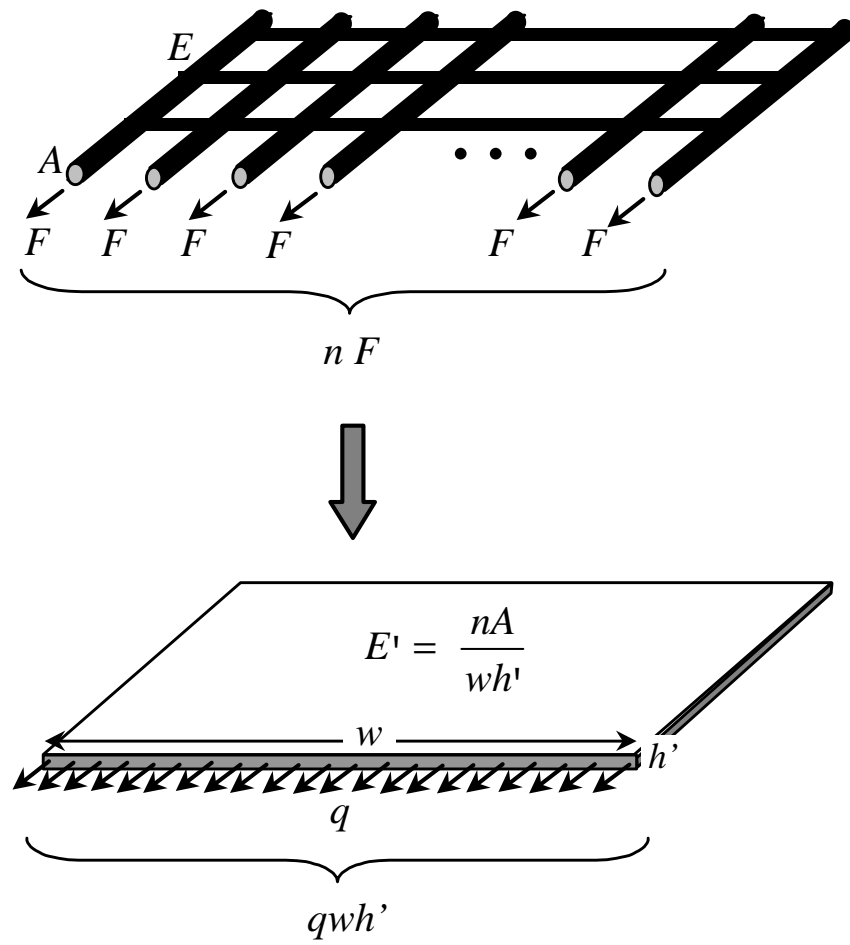


FIGURE 3 Transformed geogrid for FEM model

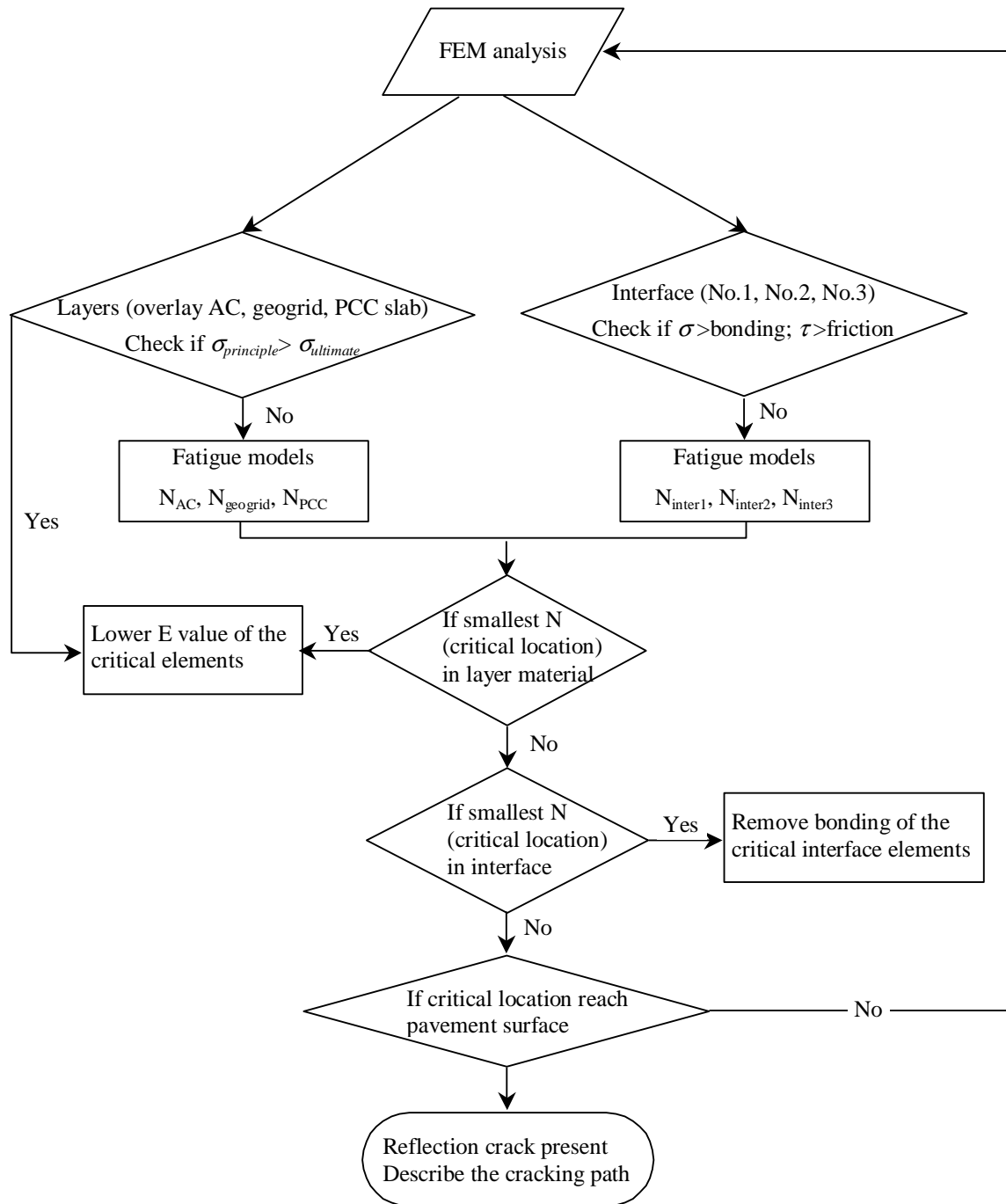
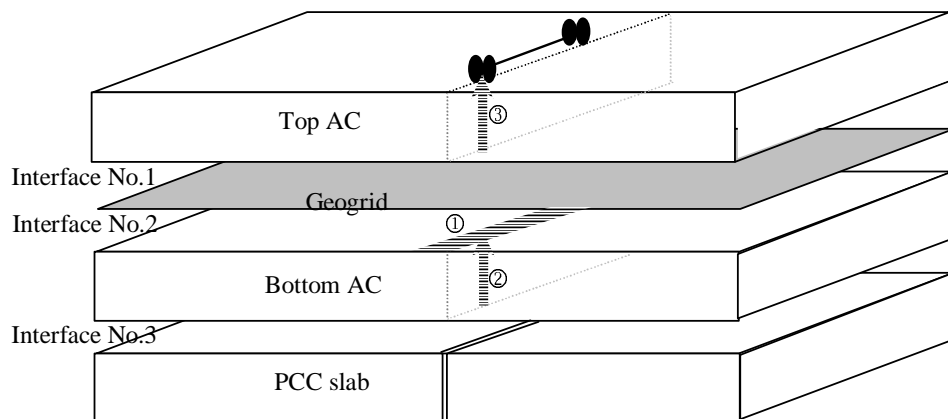
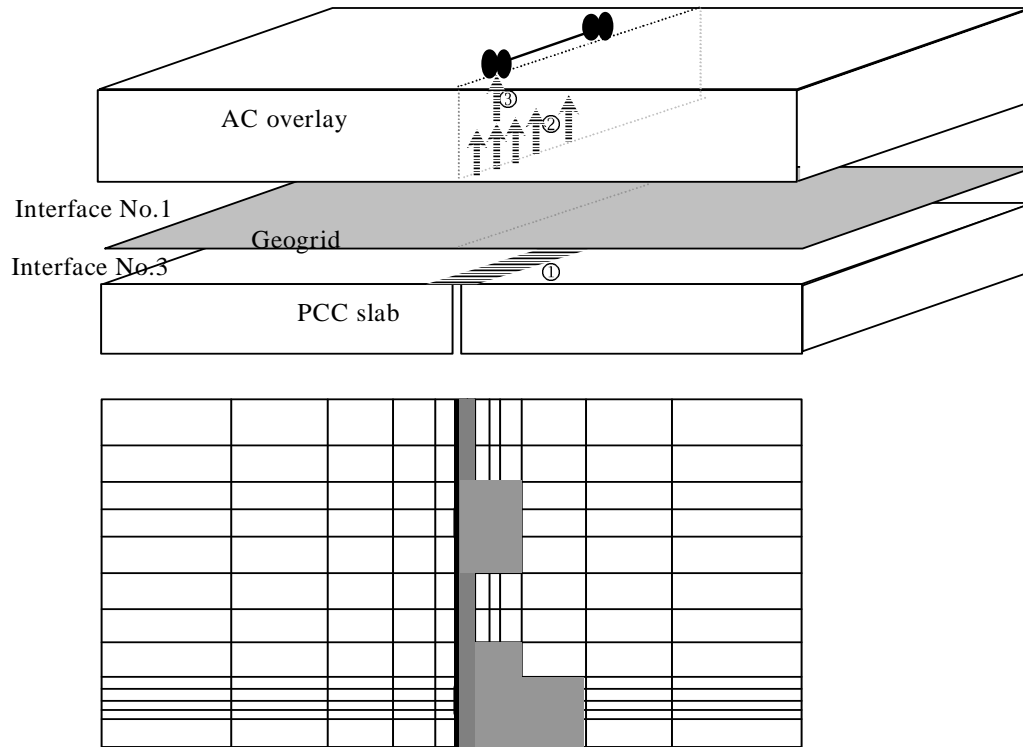


FIGURE 4 Flow chart of crack path prediction



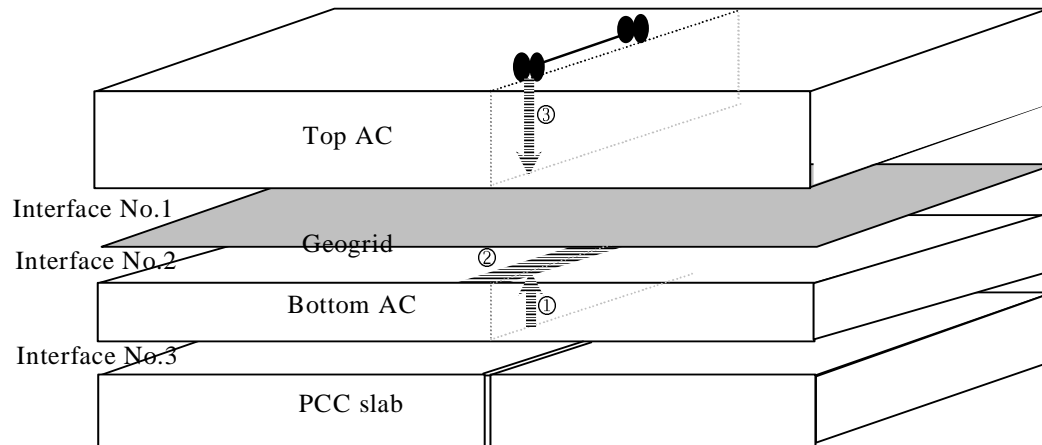
- ①: Debonding initiated at interface No.2 along the joint region
- ②: Crack developed at bottom of overlay right under the loading and propagated through the bottom layer of AC overlay
- ③: Crack continued into top overlay and reached overlay surface

FIGURE 5 Type I cracking path



- ①: Debonding initiated at interface No.3 along the joint and developed horizontally shown as shaded area.
- ②: Cracks developed at bottom of overlay right along the joint
- ③: The crack under the loading continued to penetrate the entire layer and reached overlay surface

FIGURE 6 Type II cracking path



- ①: Crack initiated at bottom of bottom overlay and propagated through the layer.
- ②: Debonding in interface No.2 along the joint.
- ③: Crack restarted at the surface of overlay and propagated downward.

FIGURE 7 Type III cracking path

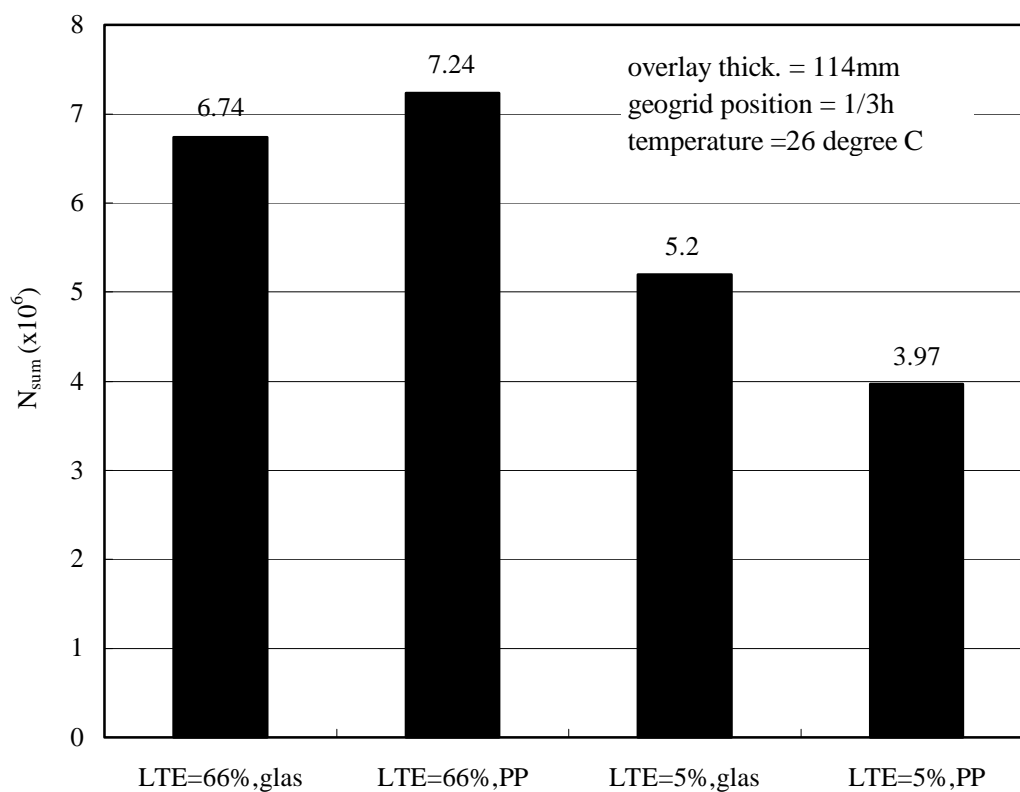


FIGURE 8 Service life comparison of Case 1, 2, 3, 4

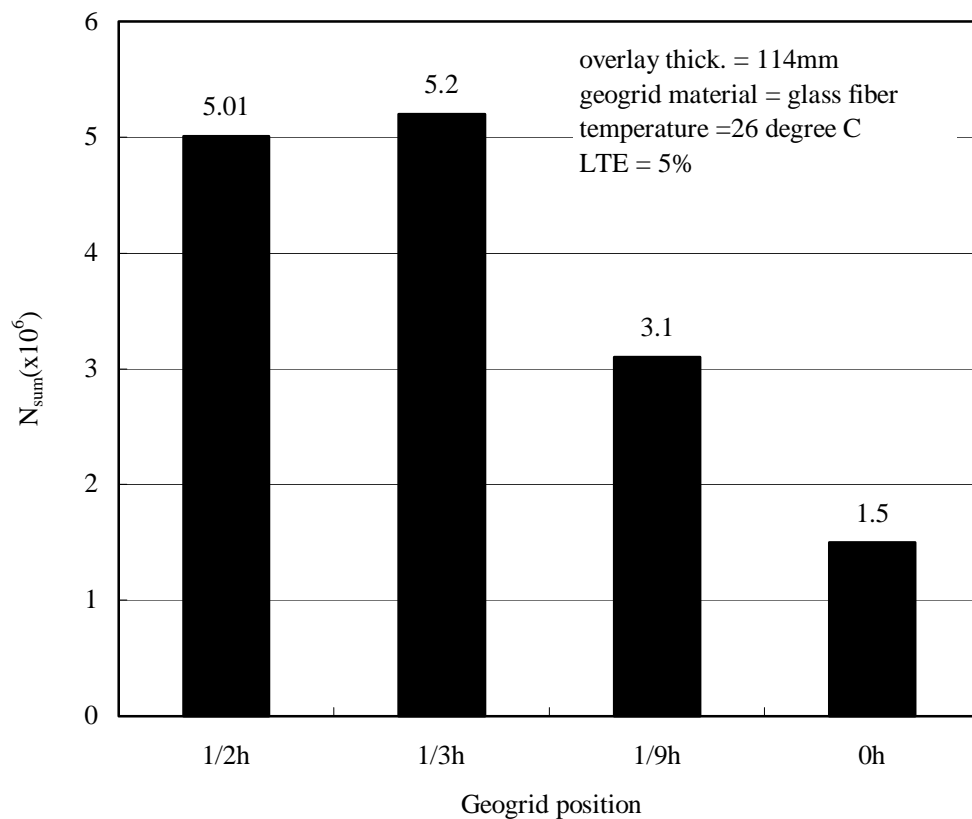


FIGURE 9 Service life comparison of various geogrid position

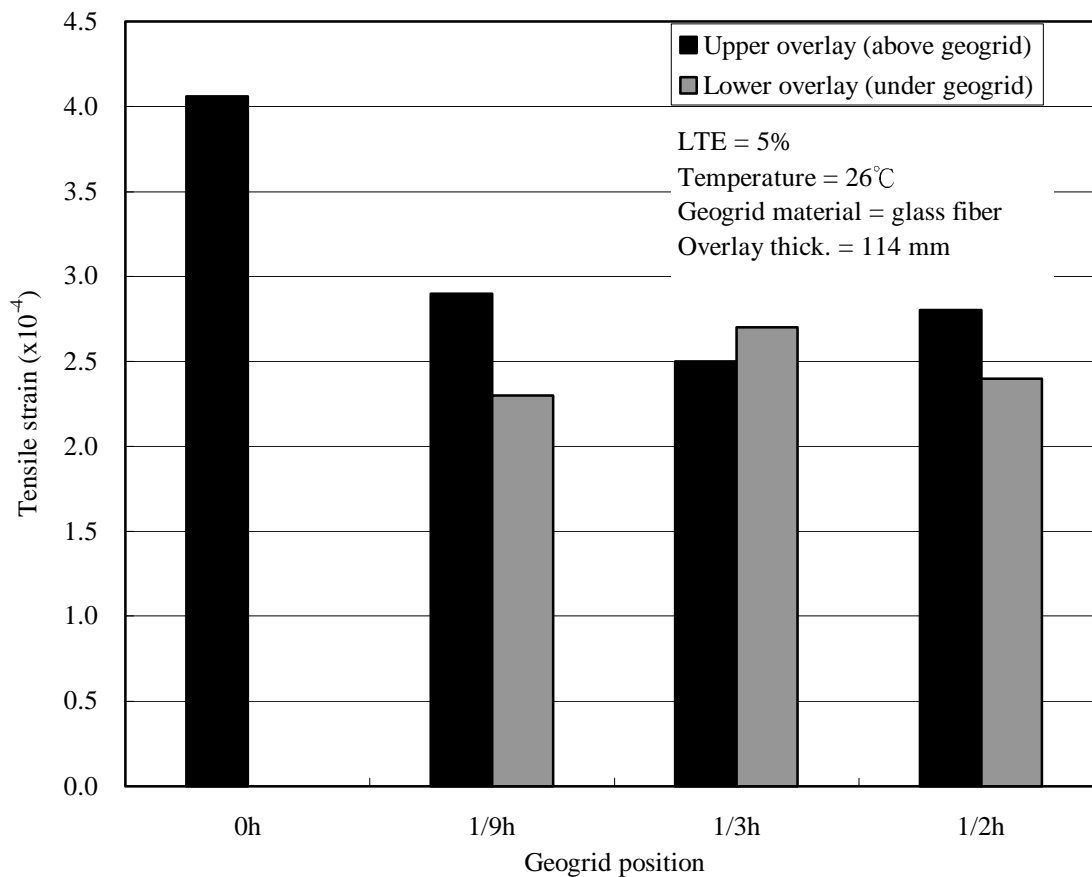


FIGURE 10 Tensile strains of various geogrid positions

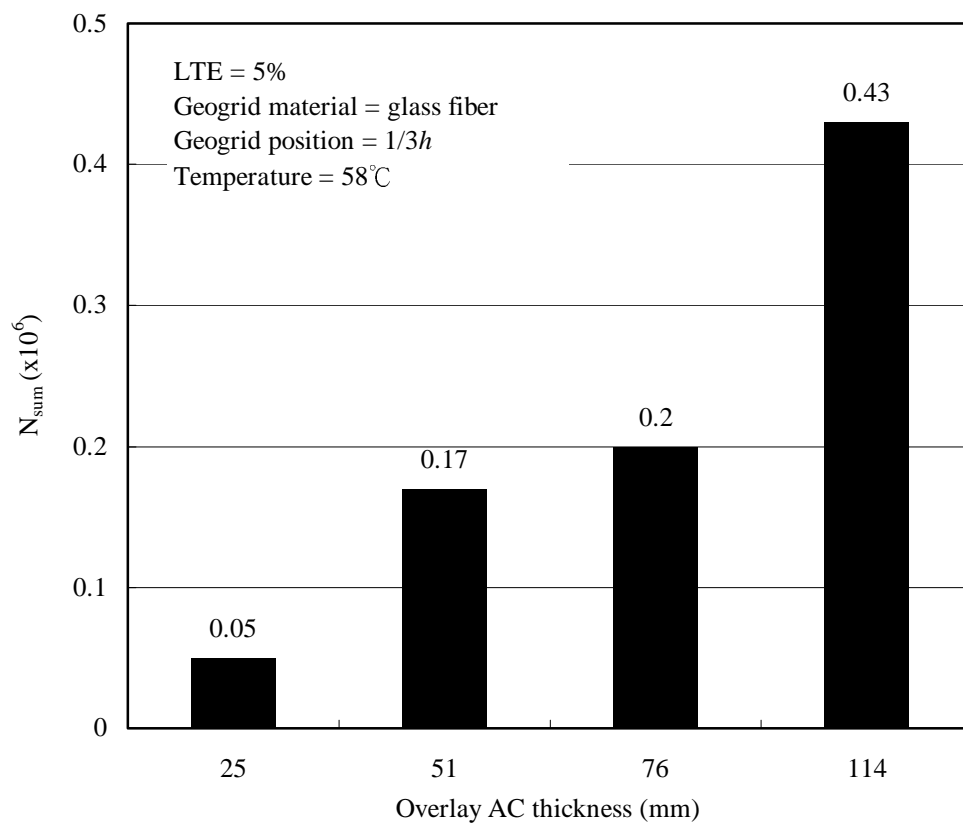


FIGURE 11 Service life comparisons of various geogrid positions

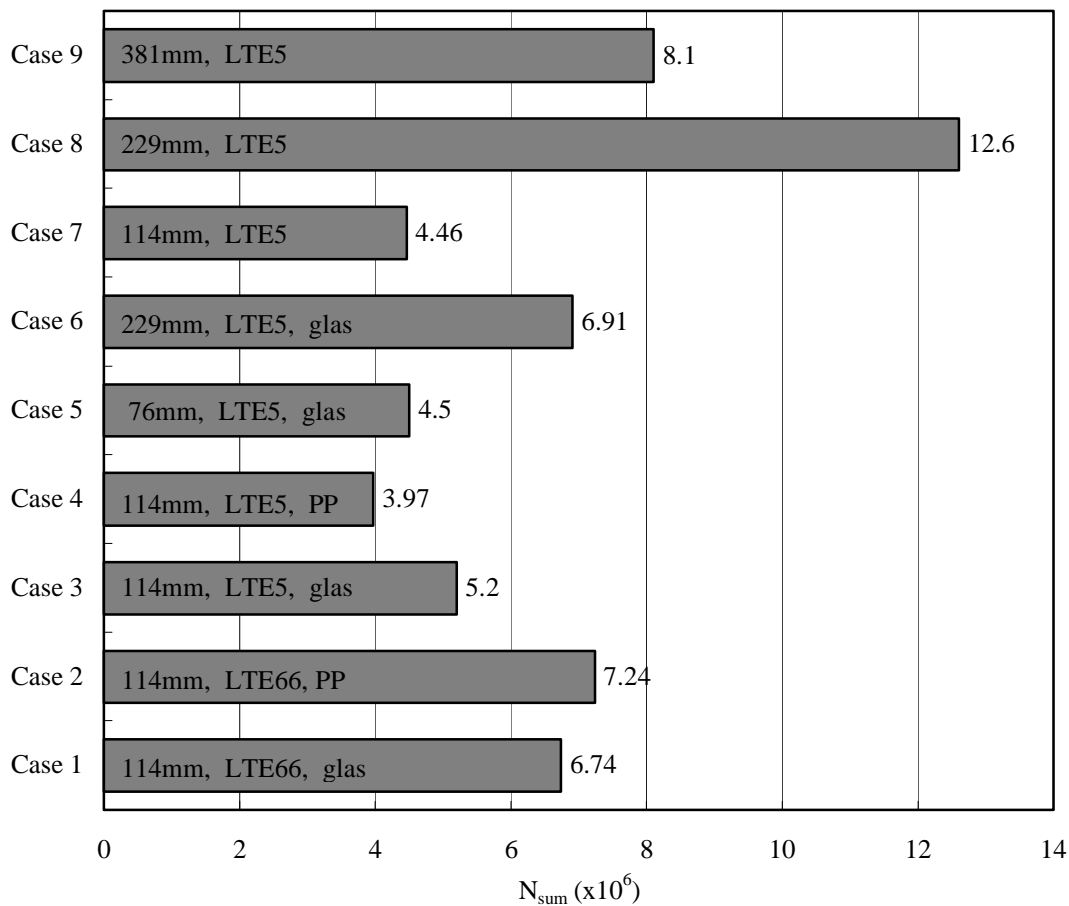


FIGURE 12 Service life comparisons of 10 analysis cases

REFERENCES

- 1 Rigo, J. M., "General Introduction, Main Conclusions of the 1989 Conference on Reflection Cracking in Pavements, and Future Prospects (1993)," *Reflective Cracking in Pavements :/State of the Art and Design Recommendations :Proceedings of the Second International RILEM Conference*, Liege, Belgium, March 10-12.
- 2 Eltahan, Ahmed A., and Lytton, Robert L. (2000), "A Mechanistic-Empirical Approach For Modeling Reflection Cracking," *Transportation Research Record*, No.1730, TRB, National Research Council, Washington, D.C., p132-138.
- 3 Rigo, J.M., Hendrick, S., Courard, L., Costa, C., Cescotto, S., and Kuck,P.J., "Evaluation of Cracking Propagation in an Overlay Subjected To Traffic and Thermal Effects (1993)," *Reflective Cracking in Pavements :/State of the Art and Design Recommendations :Proceedings of the Second International RILEM Conference*, Liege, Belgium, March 10-12.
- 4 Castell, M.A., Ingraffea, A.R., and Irwin, L.H. (2000), "Fatigue Crack Growth In Pavements," *Journal of Transportation Engineering*, ASCE, Vol.126, No.4, p283-290.
- 5 Tirado, M.R., Darter, M.T., Jayawickrama, P.W., Smith, R.E., and Lytton, R.L. (1988), "The ODE Computer Program: Mechanistic-Empirical Asphalt Concrete Overlay Design," *Transportation Research Record*, No.1207, TRB, National Research Council, Washington, D.C., pp. 30-38.
- 6 Uhlmeier, J. S., Pierce, L. M., Willoughby, K., and Mahoney, J. P. (2000), "Top-Down Cracking in Washington State Asphalt Concrete Wearing Courses," presented in 79th Annual Meeting of Transportation Research Board, Washington D.C.
- 7 Sha, Qing-Lin (1993), "Two kinds of Mechanism of Reflective Cracking," *Reflective Cracking in Pavements :/State of the Art and Design Recommendations :Proceedings of the Second International RILEM Conference*, Liege, Belgium, March 10-12.
- 8 Jenner,C.G. (1996), "Polymer Geogrid Reinforcement Construction," Proceeding of International Symposium on Geosynthetics, Shanghai, China, p139-144.
- 9 Jayawickrama, P.W., Smith, R.E., Lytton, R.L. and Tirado, M.R. (1987), *Development of Asphalt Concrete Overlay Design Equations*, Texas Transportation Institute, USA.
- 10 Guo, Zhongyin, and Zhang, Quancai (1993), "Prevention of Cracking Progress of Asphalt Overlayer With Glass Fabric," *Reflective Cracking in Pavements :State of the Art and Design Recommendations: Proceedings of the Second International RILEM Conference*, Liege, Belgium, March 10-12.
- 11 Fujio Yuge, Masahiko Ishitani, Atsushi Kasahara, and Hiroshi Kubo (1993), "Prevention of Reflection Cracking in Asphalt Overlay on Concrete Pavement with GlassGrids," *Proceedings, Paving in Cold Area Workshop*, Vol 5.
- 12 Kuo, Chen-Ming, Hall, K.T., and Darter, M.I. (1996), "Three-Dimensional Finite Element Model for Analysis of Concrete Pavement Support," *Transportation Research Record*, No.1505, 119-127, Transportation Research Board, National Research Council, Washington, D.C.
- 13 Kuo, C.-M. and Chou, F.-J., "Development of 3-D Finite Element Model of Flexible Pavements," *Journal of Transportation Engineering*, ASCE (Accepted)
- 14 Kuo, C.-M., and Jen, Ray-Wen, (2001), "The Behavior of Reinforced Asphalt Overlay on Concrete Pavements," *Journal of the Chinese Institute of Civil and Hydraulic Engineering*, Vol.13, No.4, p.839-846. (in Chinese)
- 15 Tsai, C.-F. (1995), *Study of Fatigue Characteristic of Modified and Reinforced Asphalt Concrete*, Master degree thesis, National Central University. (in Chinese)
- 16 Majizadeh, K. (1988), "A Mechanistic Approach to Rigid Pavement Design," *Concrete Pavements*, Transportation Research Board, National Research Council, p11-56.
- 17 Mandell, J. F. (1978), "Fatigue Behavior of Fibre-Resin Composites," *Developments in Reinforced Plastics*, Vol.2, p.67-107.
- 18 Wang, Y.H. (1998), *Study of Fatigue Life of Reinforced Asphalt Concrete*, Master degree thesis, Chung Yuan University. (in Chinese)
- 19 Wu, C.-L., Lue, D.-M. (1999), "Design and Performance of Ultra-thin Whitetopping Pavements," *Proceedings of 10th Conference of Pavement Engineering*, Aug.23-24, Keelung, Taiwan, p171-197